Supporting Information

A Highly Stable High-Energy Layered Oxide Cathode for Re-chargeable Sodium Ion Batteries

Ting Li[a], Yangyang Zhang[a], Yushuo Zhang[b], Xingde Xiang[a]*, Song Liu[b]*, and Chunxia Chen[b]*

Experimental section

The NLNMTO material was prepared by a traditional sol-gel method. A precursor solution was firstly prepared by dissolving 4.625 mmol $Ni(CH_3COO)_2{\cdot}4H_2O$ (Aladdin, 99.9%), 2.6875 mmol $Mn(CH_3COO)_2{\cdot}4H_2O$ (Kermel, 99.9%), 0.25 mmol $CH_3COOLi{\cdot}2H_2O$ (Kermel, 99.9%), 10.5 mmol CH_3COONa (Aladdin, 99.0%), and 10 mmol citric acid (Aladdin, 99.5%) into 30 mL distilled water, followed by adding 4 mL ethanol solution containing 2.4375 mmol isopropyl titanate. The solution was stirred at room temperature for 2 h and then evaporated at 80 °C until a gel was obtained. The gel was further dried at 120 °C in the oven for 10 h. After being sufficiently milled, the powder was heated at 600 °C for 4 h and calcined at 1000 °C for 12 h. The $NaNi_{1/2}Mn_{1/2}O_2$ and Ti-doped $NaNi_{1/2}Mn_{1/4}Ti_{1/4}O_2$ materials were prepared by the same synthesis method mentioned above, but the difference lies in whether isopropyl titanate and lithium acetate are added to the precursor solution.

Crystal structure of the material was confirmed with X-ray diffraction (XRD, X'Pert Powder with a Cu Kα radiation source), and XRD patterns were recorded in the angle range of 10-80° at a scanning rate of 8° min^{-1}. Morphologies of the materials was investigated using scanning electron microscopy (ZEISS Gemini 300) and transmission electron microscope (Japan JEOL, JEM-F200). The molar ratio of elements in the material was studied by Inductively-coupled plasma analysis (ICP-OES: Thermo Fisher iCAP PRO). Oxidation states of elements in the material was analysed by X-ray photoelectron spectroscopy (Thermo Scientific K-Alpha spectrometer equipped with an Al Kα achromatic X-ray source).

Before electrochemical measurements, working electrode was fabricated by mixing active material, conductive agent (Super P), and poly(vinyl difluoride) (PVDF) binder as a weight ratio of 7: 2: 1. The loading mass of active material in electrodes was 2.0–3.0 mg cm^{-2}. CR2032 coin-type cells was assembled in an argon-filled glove box (H_2O, O_2 < 0.1 ppm) with the working electrode, sodium sheet as counter electrode, glass fiber (Whatman, GF/F) as separator, and 1 M $NaClO_4$/EC-PC (1:1, 5wt% FEC) as electrolyte. Charge/discharge measurements were performed on a Land test system (CT2001A) in the potential range of 1.5–4.2 V. Galvanostatic intermittent titration technique (GITT) was carried out by alternately charging 10 min and resting 30 min at the current of 10 mA g^{-1}. Electrochemical workstation (VERSASTAT4) was used to carry on cyclic voltammetry at a scan rate of 0.1 mV s^{-1}. The electrochemical impedance spectroscopy (EIS) was measured on the electrochemical workstation (VERSASTAT4), with a perturbation potential of 10 mV in the frequency range of 10 kHz and 10 mHz.

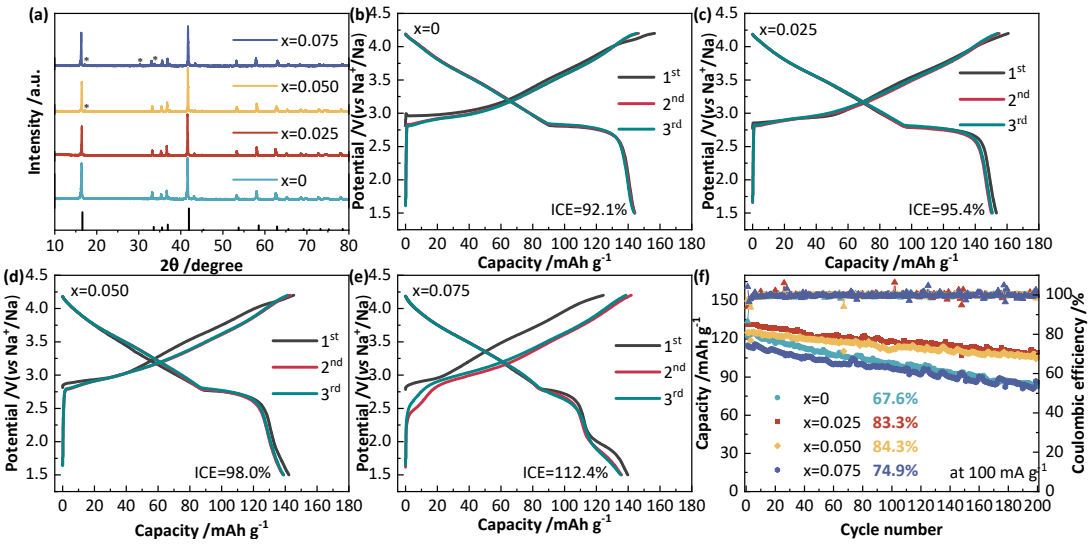

Figure S1. (a) XRD, (b-e) Galvanostatic charge/discharge profile at the current of 10 mA g^{-1}, (f) Cycling performance of $NaLi_xNi_{(1/2-3x/2)}Mn_{(1/4+3x/4)}Ti_{(1/4-x/4)}O_2$ ($0 \le x \le 0.1$) materials.

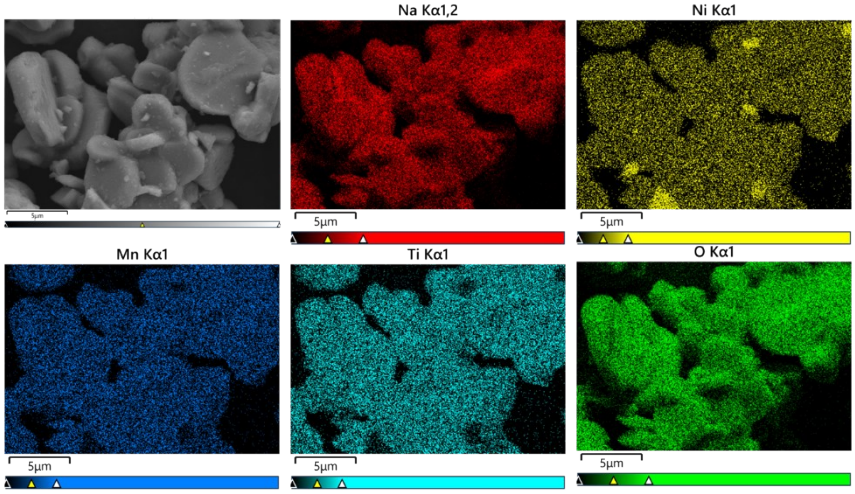

Figure S2. EDS mapping of the NLNMTO material

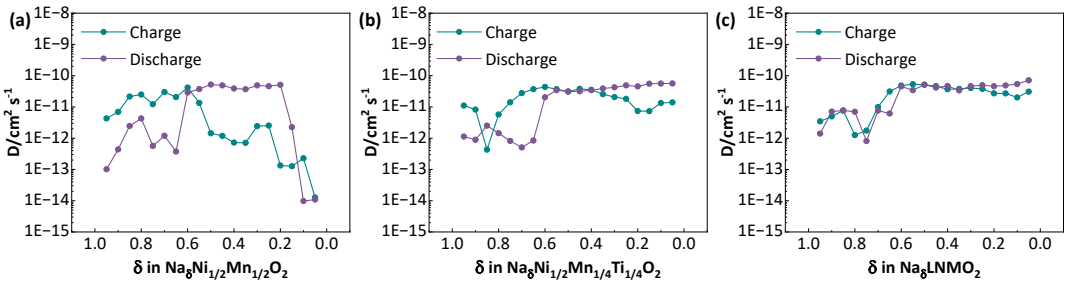

Figure S3. Apparent diffusion coefficients of Na^+ ions of (a) NNMO, (b) NNMTO and (c) NLNMTO electrodes

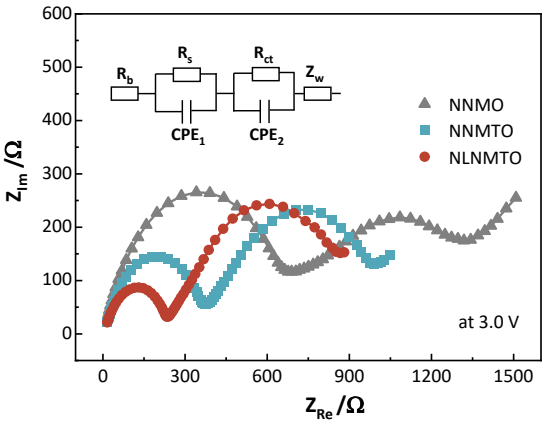

Figure S4. EIS spectra of NNMO, NNMTO and NLNMTO electrodes at 3.0 V.

Table S1. The value of R_f and R_{ct} calculated from Figure S4

electrode	$R_f(\Omega)$	$R_{ct}(\Omega)$
NNMO	748.0	754.7
NNMTO	411.4	827.3
NLNMTO	266.9	826.1

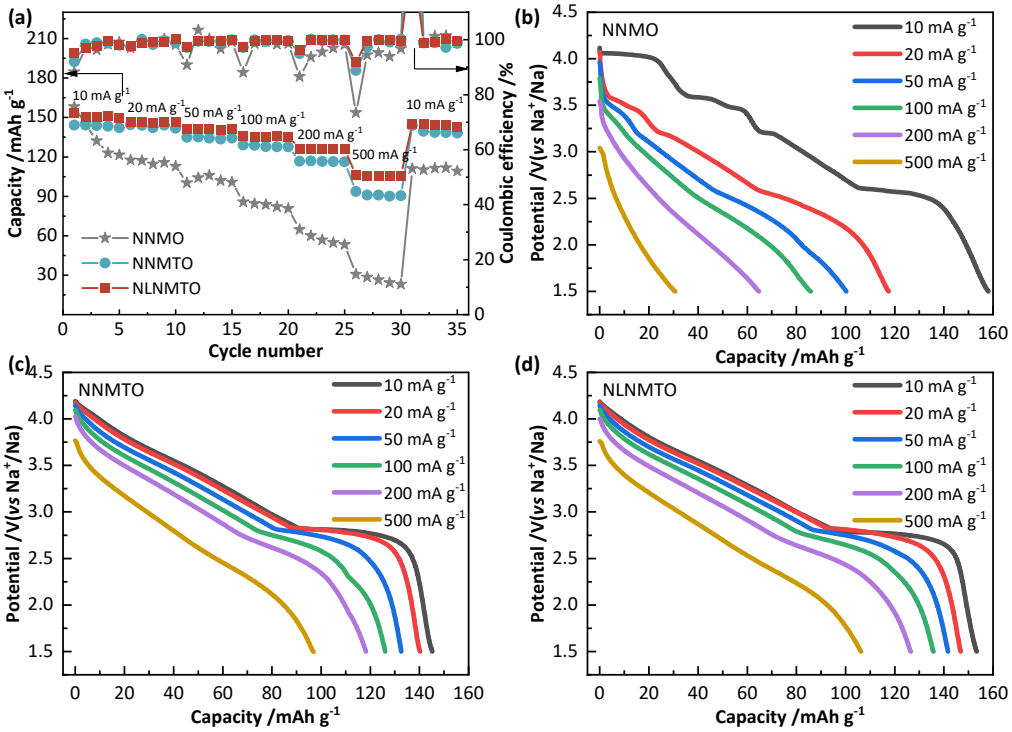

Figure S5. Rate performance of NNMO, NNMTO and NLNMTO electrodes.

Table S2. Performance comparison of our material and reported cathode materials

Materials	Capacity (mAh g^{-1})	Capacity retention
$Na_{0.993}Ni_{0.382}Mn_{0.428}Cu_{0.098}Sn_{0.049}O_2$[1]	115.3 at 50 mA g^{-1}	80.7% after 500 cycles
$NaNi_{0.45}Al_{0.1}Mn_{0.45}O_2$[2]	105 at 17 mA g^{-1}	86.2% after 200 cycles
$Na_{0.9}Ni_{0.2}Fe_{0.2}Co_{0.2}Mn_{0.2}Ti_{0.15}Cu_{0.05}O_2$[3]	117.8 at 22 mA g^{-1}	70.7% after 1000 cycles
$NaCu_{0.1}Ni_{0.3}Fe_{0.2}Mn_{0.2}Ti_{0.2}O_2$[4]	130.0 at 13 mA g^{-1}	71% after 500 cycles
$Na_{0.93}Li_{0.12}Ni_{0.25}Fe_{0.15}Mn_{0.48}O_2$[5]	130.1 at 40 mA g^{-1}	82.8% after 200 cycles
$NaNi_{0.25}Fe_{0.455}Al_{0.045}Mn_{0.25}O_2$[6]	131.7 at 24 mA g^{-1}	81.6% after 100 cycles
$NaNi_{1/3}Fe_{1/3}Mn_{1/3}O2$[7]	135.0 at 12 mA g^{-1}	80% after 300 cycles
$NaNi_{0.5}Mn_{0.45}Sn_{0.05}O_2$[8]	126.1 at 12 mA g^{-1}	76.2% after 450 cycles
$NaFe_{0.2}Cu_{0.1}Ni_{0.2}Mn_{0.3}Ti_{0.2}O_2$[9]	121.0 at 10 mA g^{-1}	83.8% after 200cycles
$NaFe_{0.2}Co_{0.2}Ni_{0.2}Ti_{0.2}Sn_{0.1}Li_{0.1}O_2$[10]	112.7 at 10 mA g^{-1}	81% after 100cycles
$NaNi_{0.3}Fe_{0.4}Mn_{0.3}O_2$[11]	124.0 at 24 mA g^{-1}	76% after 100cycles
This work	153.1 at 10 mA g^{-1}	83% after 200cycles

1. Liang Z, Ren M, Guo Y, et al. Depressed P3–O3' Phase Transition in an O3-Type Layered Cathode for Advanced Sodium-Ion Batteries [J]. Inorganic Chemistry Frontiers, 2023, 10(24): 7187-7192.
2. Peng B, Chen Y, Zhao L, et al. Regulating the Local Chemical Environment in Layered O3-$NaNi_{0.5}Mn_{0.5}O_2$ Achieves Practicable Cathode for Sodium-Ion Batteries [J]. Energy Storage Materials, 2023, 56: 631-641.
3. Wang X Z, Zuo Y, Qin Y, et al. Fast Na^+ Kinetics and Suppressed Voltage Hysteresis Enabled by a High-Entropy Strategy for Sodium Oxide Cathodes [J]. Advanced Materials, 2024.
4. Lin C C, Liu H Y, Kang J W, et al. In-Situ X-ray Studies of High-Entropy Layered Oxide Cathode for Sodium-Ion Batteries [J]. Energy Storage Materials, 2022, 51: 159-171.
5. Yuan X G, Guo Y J, Gan L, et al. A Universal Strategy toward Air-Stable and High-Rate O3 Layered Oxide Cathodes for Na-Ion Batteries [J]. Advanced Functional Materials, 2022, 32(17): 11.
6. Feng Y H, Cheng Z W, Xu C L, et al. Low-Cost Al-Doped Layered Cathodes with Improved Electrochemical Performance for Rechargeable Sodium-Ion Batteries [J]. Acs Applied Materials & Interfaces, 2022, 14(20): 23465-23473.
7. Gao X, Wang H J, Liu H Q, et al. Post-Substitution Modulated Robust Sodium Layered Oxides [J]. Small Methods, 2023: 2300635.
8. Hu H Y, Wang H R, Zhu Y F, et al. A Universal Strategy Based on Bridging Microstructure Engineering and Local Electronic Structure Manipulation for High-Performance Sodium Layered Oxide Cathodes [J]. Acs Nano, 2023, 17(16): 15871-15882.
9. Dang Y Z, Xu Z, Yang H D, et al. Designing Water/Air-stable Co-Free High-Entropy Oxide Cathodes with Suppressed Irreversible Phase Transition for Sodium-Ion Batteries [J]. Applied Surface Science, 2023, 636: 157856.
10. Tian K H, He H, Li X, et al. Boosting Electrochemical Reaction and Suppressing Phase Transition with a high-entropy O3-type layered oxide for sodium-ion batteries [J]. Journal of Materials Chemistry A, 2022, 10(28): 14943-14953.
11. Lamb J, Jarvis K, Manthiram A. Molten-Salt Synthesis of O3-Type Layered Oxide Single Crystal Cathodes with Controlled Morphology towards Long-Life Sodium-Ion Batteries [J]. Small, 2022, 18(43): 2106927.